High-Precision Radiometric Tracking for Planetary Approach and Encounter in the Inner Solar System

C. S. Christensen and S. W. Thurman
Navigation Systems Section

J. M. Davidson, M. H. Finger, and W. M. Folkner
Tracking Systems and Applications Section

The benefits of improved radiometric tracking data have been studied for planetary approach within the inner Solar System using the Mars Rover Sample Return trajectory as a model. It was found that the benefit of improved data to approach and encounter navigation was highly dependent on the a priori uncertainties assumed for several non-estimated parameters, including those for frame-tie, Earth orientation, troposphere delay, and station locations. With these errors at their current levels, navigational performance was found to be insensitive to enhancements in data accuracy. However, when expected improvements in these errors are modeled, performance with current-accuracy data significantly improves, with substantial further improvements possible with enhancements in data accuracy.

I. Introduction

An investigation of the benefits of improved radiometric tracking data for interplanetary navigation has been initiated. The goals are to determine the limitations imposed on navigation performance by radiometric data accuracy and how to best utilize this high-accuracy data to optimize navigation performance. For this purpose, covariance analyses using the Orbit Determination Program (ODP) have been performed, including two-way Doppler, two-way range, and Delta Differenced One-way Range (ΔDOR) measurements with various assumed accuracies for each data type. Three sets of results are presented, with the Mars Rover Sample Return (MRSR) Mission cruise and encounter trajectory used as a model for each set.[1,2]

Since only a single trajectory has been studied, some caution is needed in generalizing the results. In particular, the

[1] A. Konopliv, "Cruise Navigation Analysis for MRSR with Radiometric Data Only," JPL IOM 314.4-608 (internal document), Jet Propulsion Laboratory, Pasadena, California, December 2, 1987.

[2] A. Konopliv, "MRSR Approach Navigation–More Results for Radiometric and Optical Data," JPL IOM 314.4-621 (internal document), Jet Propulsion Laboratory, Pasadena, California, April 7, 1988.

ephemeris of Mars is the best known of all the planets (excluding Earth), so that this study may present the most favorable case. Also note that for this model trajectory, encounter takes place when Mars is near its most southerly declination. An encounter lying closer to the celestial equator might affect the impact of Doppler data on the total orbit determination accuracy, and a trajectory lying in the northern sky might give added strength to the ΔDOR measurements because of the increased visibility on the Goldstone/Spain baseline. However, it is expected that the effects of these variations on the studies presented in this work will be either minor, since the impact of Doppler data is generally limited, or possibly beneficial, since the impact of ΔDOR data is strongly positive.

For the first set of results (solution set number one), the ephemeris and station location a priori uncertainties used are appropriate for the present time and near future (i.e., 1988–1990). A simple equivalent station location error (ESLE) approach was adopted, in which a priori uncertainties in Earth orientation and troposphere are lumped together with the station location uncertainties to give one "equivalent" station location covariance which accounts for the errors in all three quantities. For these runs, the ESLE and ephemeris errors were considered as unestimated systematic errors. In the covariance analysis results, the considered ephemeris errors made the dominant contribution to the total orbit determination uncertainty for nearly all combinations of data. Also, it was found that for improved range and Doppler accuracy the ESLE contribution to the orbit determination uncertainty grew in size, causing the total uncertainty to increase as data became more accurate. These results were not unexpected, but they are presented here to serve as a benchmark for comparison with later runs.

For solution set number two, the a priori ephemeris covariance of set one was replaced by another in which it had been assumed that the right ascension offset between the dynamical reference frame of the planets and the Very Long Baseline Interferometry (VLBI) quasar frame had been established at the level of 5 nanoradians. This step resulted in an ephemeris with an a priori frame tie error of about 5 nanoradians in each of the three rotational directions. In addition, the ESLE approach was abandoned and replaced by a more physically realistic one in which station location and troposphere errors are considered independently and in which Earth orientation parameters are estimated stochastically. All a priori uncertainties used, except for that of the ephemeris, were the same as in solution set one. It was found that the contributions of ephemeris and station errors to the orbit determination uncertainty decreased significantly and that the total uncertainties (compared to those of solution set one) were smaller by factors of up to eight, depending on the combination of observables and accuracies assumed.

Solution set three differs from solution set two in that new a priori errors for station location, troposphere, and Earth orientation parameters are adopted, representing higher levels of accuracy for these calibrations, as should be available in the mid- to late 1990s. These results showed that orbit determination uncertainties could be decreased by an additional 10–60 percent (compared to those of set two), again depending on the combination of observables and accuracies assumed.

The results from the analyses described above suggest that orbit determination for missions to the inner planets will benefit most significantly from an improved determination of the tie between the dynamical frame of the planets and the inertial frame of the quasars. There is a reasonable hope of determining this tie for the inner planets at the level of 5–10 nanoradians within the next few years. Promising measurement techniques include improved ground surveys linking key Lunar Laser Ranging (LLR) and VLBI sites,[3] VLBI observations of short-period pulsars [1], observations of planetary occultations of quasars,[4] and VLBI measurements during the Phobos Lander Mission[5] and the Mars Orbiter Mission.

With this frame tie established, further advances in orbit determination accuracy can result from improved radiometric data. Achieving the full benefit of more accurate data will require two additional efforts. First, improvements in modeling are required. Station location, troposphere, and Earth orientation errors need to be given a physically realistic representation, with separate parameters and partial derivatives provided for each. Second, improvements in calibration are required. Reductions in the present a priori errors for station locations, troposphere delays, and Earth orientation will significantly enhance orbit determination with high-accuracy radiometric data types. These calibration improvements are expected to be achieved through advances in VLBI and GPS technology.

Once these improvements are implemented, navigational performance for cruise and encounter to the inner planets will benefit significantly from improved radiometric data. For these mission scenarios, improvement in the accuracy of ΔDOR observables has the greatest effect on spacecraft posi-

[3] A. E. Niell, "Absolute Geocentric DSN Station Locations and Radio-Planetary Frame Tie," JPL IOM 335.2-159 (internal document), Jet Propulsion Laboratory, Pasadena, California, March 21, 1984.

[4] R. Linfield, "The Need for DSS-43 on July 19, 1988 for a Venus Occultation," JPL IOM 335.3-88-51 (internal document), Jet Propulsion Laboratory, Pasadena, California, April 25, 1988.

[5] C. E. Hildebrand, "First Cut at Phobos Lander VLBI Errors," JPL IOM 335.1-87-29 (internal document), Jet Propulsion Laboratory, Pasadena, California, February 3, 1987.

tional covariances at encounter. Improving the ΔDOR accuracy from 50 nrad to 5 nrad was found to reduce orbit determination uncertainties by a factor of three when the ΔDOR data was used in conjunction with 10-m range and 1-mm/sec Doppler. Improvements in range and Doppler accuracy can be beneficial, but in general will have a more limited effect, except in the absence of ΔDOR data. In this regard, 10-cm accuracy range proves to be a powerful stand-alone data type, producing results superior to those achievable with the 10-m range, 1-mm/sec Doppler, and 50-nrad ΔDOR data type combination.

II. Trajectory and Observation Schedule

The three sets of results presented here are based on the Mars Rover Sample Return (MRSR) Mission approach trajectory discussed by A. Konopliv.[6] With this trajectory the spacecraft encounters Mars on October 7, 1999. All the orbital solutions presented are based on a common observation schedule, which is summarized in Table 1. The first data point is taken 85 days before Mars aerocapture and the last point is taken 2 days before Mars encounter. Two-way Doppler and two-way range were scheduled from the three stations DSS-11, DSS-44, and DSS-61. Doppler and range data were scheduled from each station for one pass every sixth day, with stations alternating so that a pass was scheduled somewhere for every other day. A minimum spacecraft elevation of 10 deg was required for this data. A one-hour integration time was used for Doppler data, while range measurements were scheduled approximately every hour within a pass. The ΔDOR measurements on the DSS-11–DSS-44 and DSS-11–DSS-61 baselines were scheduled once every sixth day with quasars selected to be within 10 deg of the spacecraft. ΔDOR data below 5-deg elevation was eliminated. The total amount of data scheduled was 309 Doppler points, 296 range points, and 28 ΔDOR points.

III. Estimation Strategy and Error Modeling Common to All Solutions

The covariance analyses were performed with the ODP using batch sequential estimation. A batch time interval of one day was used in all cases. This was chosen to be small compared to the correlation time constants of all stochastically estimated variables. For all runs, estimated parameters include those for spacecraft initial state, solar pressure, and a random nongravitational acceleration. Considered parameters include those for a constant nongravitational acceleration, Mars GM and J2, and quasar directions. The error modeling common to all solutions will be discussed in this section and is summarized in Table 2. Modeling specific to solutions sets one, two and three are summarized in Tables 3, 4, and 5 respectively, and will be discussed in later sections.

Since the interest is in the effects of data accuracy on orbit determination accuracy, the initial position and velocity of the spacecraft were estimated with large a priori uncertainties of 10,000 km for each position coordinate and 1 km/s for each velocity component. These large values were chosen so that the final state determination would not be dependent on the a priori values.

A solar pressure model was included. This model assumes that the spacecraft has a mass of 1000 kg and presents an area of 17 m^2 toward the Sun. The solar pressure force is calculated as the force on an opaque body with this projected area times a reflectivity vector $\vec{G}$. The components of $\vec{G}$ are assumed to be constant in a coordinate system defined by the Sun-spacecraft and Sun-Canopus directions. The component of $\vec{G}$ directed away from the Sun, G_r, was estimated with an a priori uncertainty of 0.13, while the components of $\vec{G}$ perpendicular to the Sun-spacecraft direction, G_x and G_y, were each estimated with an a priori uncertainty of 0.01. This modeling is the same as used by Konopliv.

To account for other non-gravitational forces, both stochastic and constant accelerations were employed. Stochastic accelerations of 10^{-12} km/sec^2 per component were estimated with a 5-day correlation time. Constant accelerations with a priori uncertainties of 10^{-12} km/sec^2 per component were considered.

To account for uncertainties in the Martian gravity field, the GM and J2 of Mars were considered with uncertainties of 0.15 km^3/sec^2 and 4.4×10^{-7}, respectively. Although these uncertainties are 10 times the formal errors, their effects on the orbit determination accuracy are never very significant.

The philosophical viewpoint has been taken that the fundamental reference frame for navigation is that determined by the quasars. It is believed that this allows the simplest representation of errors in orientation between the radio frame, the terrestrial reference frame, and the dynamical reference frame of the ephemerides. Presently the quasar catalog is internally consistent at the 5- to 10-nrad level [2]. Therefore, independent 5-nrad per component errors for each quasar direction have been considered.

Each solution set consists of ODP runs performed with different combinations of data types and accuracies. Data accuracies used were 30 cm or 3 cm for the ΔDOR, corresponding to about 50- or 5-nrad angular uncertainty, 1000 m, 10 m, or or 0.1 m for the range, and 1.0 mm/sec or 0.01 mm/sec for

[6] See Footnotes 1 and 2.

the Doppler. Runs were made with all possible combinations of these data accuracies. Runs were also made with ΔDOR and range only, ΔDOR and Doppler only, range and Doppler only, ΔDOR only, Doppler only, and range only. This led to a total of 35 runs for each solution set.

IV. Solution Set One

A. Error Modeling

Solution set one represents a first cut at investigating the dependence of orbit determination accuracy on radiometric data accuracy. For this set, relatively simple extrapolations of present day estimates of the errors for the ephemeris, the station locations, and other error sources were adopted. The results of this first solution set provided the information necessary to focus on the important error terms and neglect largely irrelevant terms. The error models particular to solution set one are summarized in Table 3.

The ephemeris errors used were supplied by M. E. Standish of the Navigation Systems Section in the form of a joint Earth–Mars set-III parameter covariance matrix. This ephemeris covariance represents the formal calculated errors appropriate for a modern ephemeris. These formal errors are often multiplied by a scale factor of two to five to make a crude allowance for systematic error. However, examination of the covariance matrix shows that the dominant component of error consists of a 100-nrad uncertainty in the zero point of right ascension for the ephemeris. All other orientation components of the ephemeris covariance are on the order of 5 nrad. Since the radio frame has been adopted as the fundamental frame for navigation, this right ascension uncertainty should correspond to the major component of the frame tie error between the planetary frame and the radio frame. The 100-nrad value for this uncertainty is consistent with the current estimate of the planetary-radio frame tie error for the inner planets [3, 4]. Therefore, the ephemeris errors are considered with no scaling. By doing so, the present frame-tie error is correctly modeled, but errors for the internal consistency of the ephemeris that are at present too small may be incorporated.

For solution set one the common "equivalent station location error" (ESLE) approach was adopted in which geocentric station coordinate, Earth orientation, and media calibration errors are lumped together into a single set of effective station errors. Present VLBI measurements establish Deep Space Network (DSN) baselines to 10 cm in the radio frame [5]. Geocentric station locations can potentially be derived from these baselines and Global Positioning System (GPS) satellite tracking data [6] with errors on the level of 10 cm. Therefore, 10-cm per component errors for the geocentric station coordinate contribution to the ESLEs have been used.

Due to unmodelable changes in the Earth's rotation rate and pole location, accurate information about the orientation of the Earth can be obtained only through a constant monitoring program. The largest component of error is in UT1-UTC, an offset in right ascension. The JPL Time and Earth Motion Precision Observations (TEMPO) deliveries for Magellan are expected to have a worst case (10-day extrapolation) UT1-UTC error of 50 nrad.[7] This error has been accounted for by adding to the station location a priori covariance matrix a 50-nrad longitude error, fully correlated between stations.

For the media errors it was assumed that dual-frequency tracking could be used to calibrate out the ionosphere error and that the 4-cm wet troposphere error [7] derived from using monthly averages would not contribute significantly to the equivalent station location error. Hence, for solution set one ionosphere and troposphere errors were not explicitly included.

B. Results

To compare the results for the large number of combinations of data accuracies employed here, most results are presented in the form of root-sum-squared (RSS) position uncertainties at the nominal time of closest approach to Mars. In contrast, the critical navigational requirement of MRSR delivery is control of the angle of atmospheric entry. The RSS position error was chosen as a figure of merit over the more mission-specific angle of entry because it was felt to be more generally reflective of the overall accuracy of the orbit determination. In practice it has been found that the dominant error sources affect most of the orbit parameter uncertainties, and that the general trends in changes in orbit determination uncertainty with changes in data accuracy are visible in any figure of merit.

Table 6 gives the RSS position uncertainty at closest approach for all combinations of data types and accuracies with a breakdown of the total RSS uncertainties into calculated uncertainty and the contributions from considered errors. The 35 cases are listed by the ΔDOR accuracy, Doppler accuracy, and range accuracy. The main conclusions from solution set one are demonstrated by the three cases depicted in Fig. 1. In Fig. 1 the RSS uncertainty is broken down into components for the cases which include 30-cm ΔDOR, 1-mm/sec Doppler, and 1000-m, 10-m, or 0.1-m range. The dominant contribution is due to the considered ephemeris errors and is virtually constant regardless of data accuracies.

[7] T. F. Runge, "UTPM Calibration Accuracy for Magellan," JPL IOM 335.5-87.81 (internal document), Jet Propulsion Laboratory, Pasadena, California, April 30, 1987.

The calculated uncertainty decreases with improving range accuracy, with a significant improvement between the 10-m and 0.1-m case. This is because the 0.1-m range taken over an entire pass contains angular information with an accuracy of about 0.1 m divided by the diameter of the Earth, which is competitive with the 30-cm ΔDOR accuracy and reduces the dominant plane of the sky error.

However, the consider contribution due to the equivalent station location errors increases with improved range accuracy. For the 0.1-m range case the station location contribution is larger than the calculated uncertainty and the total uncertainty is larger than for the cases with less accurate range. This behavior is due to the estimation strategy employed. The station location errors have been considered rather than estimated. The spacecraft state estimate is therefore made without accouting for these errors. The effects of the station location errors upon this suboptimal estimate are then accounted for in the consider analysis. As the range accuracy approaches the level of the equivalent station location errors, the suboptimal nature of the estimate becomes more important than the accuracy of the data. A common approach that avoids this behavior, and gains some benefit from improved data accuracy, is to deweight the more accurate range data. For example, if the 0.1-m range were treated as if it were 10-m range, then the station location uncertainty consider contribution to the total error would be the same as for the 10-m range case, but the improved data accuracy would reduce the actual error somewhat below that for the 10-m case. However, ODP has no capability to evaluate the actual error that results from this procedure. To gain the full benefit of the more accurate range will require improvements in the modeling of the error sources that have been lumped into the equivalent station location errors.

Figures 2, 3, and 4 examine the B-plane (impact parameter plane) components for the same cases used in Fig. 1. Figure 2 shows the uncertainty breakdown in $B \cdot R$ (perpendicular to the Mars orbital plane). Figure 3 shows the uncertainties in $B \cdot T$ (in the Mars orbital plane). Figure 3 shows the uncertainty breakdown for the linearized time of flight (LTOF). These figures show that the trends seen in the RSS position uncertainty figure are preserved in each component in the B-plane, with the ephemeris contribution being dominant and independent of data accuracy, and the station location contribution and the total uncertainty increasing with improved range.

V. Solution Set Two

A. Error Modeling

The orbit determination uncertainties predicted with solution set one were dominated by the considered ephemeris errors, and also, for the most accurate range or Doppler, by the equivalent station location errors. Experiments in the near future promise dramatic reductions in the planetary-radio frame-tie error. This reduction has been incorporated in the error modeling for solution set two. In addition, the equivalent station location error approach has been abandoned in favor of explicitly modeled station coordinates, Earth orientation, and troposphere errors, allowing the effects of each of these error sources to be individually examined. These changes in error modeling are summarized in Table 4.

Determination of the orientation of the dynamical reference frame of the planets relative to the VLBI quasar frame can be accomplished by several methods. One approach suggested by A. E. Niell[8] involves linking Lunar Laser Ranging (LLR) sites, which have accurate positions in the planetary frame, to the DSN network. The LLR data establish the geocentric locations of these sites to better than 10-cm accuracy.[9] These locations could be combined with VLBI-determined DSN baseline measurements (also accurate to 10 cm) to provide the frame-tie information. Previous efforts to do this have suffered from insufficient measurements relating the LLR sites to the DSN sites.[10,11] The McDonald LLR site has been accurately measured with respect to the Fort Davis VLBI site to provide one link between the frames. Fixing the LLR network to the VLBI network at one point does not determine rotations about that point however. At least one other link between the networks is needed to establish the right ascension frame tie. Recent GPS measurements of the baseline between the Haleakala LLR site and the nearby Kokee Park VLBI site may be used to provide a second link between the networks [8, 9]. This may resolve the right ascension frame tie to 5–10 nrad since the relative declination is already known to the 5-nrad level. Further measurements connecting the VLBI network to the LLR network are desirable to provide a more complete solution.

The more direct approaches to establishing the frame tie involve astronomical observations. Comparison of the directions measured to short-period pulsars by radio interferometry and the directions determined by analysis of pulse arrival times can be used to establish the orientation of the planetary

[8] See Footnote 3.

[9] X. X. Newhall, personal communication.

[10] See Footnote 3.

[11] D. Jones, "A. E. Niell's Method for Comparing DSN Station Locations to Determine Extragalactic–Planetary Frame Tie," JPL IOM (internal document), Jet Propulsion Laboratory, Pasadena, California, November 30, 1986.

frame relative to the radio frame [1]. The direction to the millisecond pulsar 1937+21 is known from timing analysis to 5 nrad relative to the Earth's orbit. At present the direction in the radio frame has only been established to 250 nrad by a VLA observation. Future VLBI observations promise greatly improved accuracy. Radio observations of the occultation of quasars by planets yield information on the frame tie. An occultation of P 0507+17 by Venus[12] has been observed, and is currently being analyzed. VLBI observations of spacecraft during encounters have established the present 100-nrad knowledge of the frame tie [3, 4]. The upcoming Phobos Lander frame-tie experiment is expected to provide a planetary-radio frame of much improved accuracy.[13] A similar experiment could be included with the Mars Observer mission to confirm the Phobos results in time for the MRSR mission.

For solution set two it has been assumed that the right ascension offset between the dynamical reference system of the planets and the VLBI quasar system has been established at the 5-nrad level. A new Earth–Mars ephemeris covariance matrix was produced by inverting the original covariance used in solution set one to obtain the information matrix, adding a 5-nrad measurement of the offset in right ascension of Earth's orbit from its nominal orbit, and reinverting. It is stressed that only an improvement in the knowledge of the orientation in right ascension of the figure of the Earth's orbit has been assumed. No new information has been added about the Earth's phase in its orbit, or about the level of errors that change the shape or period of the orbit, or that rotate the orbit about axes that lie in the plane of Earth's equator. Any improvement in the Martian ephemeris is due entirely to its existing accuracy relative to Earth's ephemeris.

The behavior of the equivalent station location errors contribution to the orbit determination uncertainty prompted us to separate the Earth orientation error from the geocentric station location errors. The Earth orientation error is random and should have signature and temporal behavior significantly different from the geocentric station coordinate offsets and deserves to be modeled explicitly. The ODP link REGRES does not generate Earth orientation partials. Code has therefore been written to include the partial derivatives for Earth orientation in the ODP REGRES file via the ODMODIFY program. The desired partials may be calculated by the chain rule:

$$\frac{\partial X}{\partial \theta_i} = \sum_{j=1}^{3} \left[\frac{\partial X}{\partial u_j} \frac{\partial u_j}{\partial \theta_i} + \frac{\partial X}{\partial v_j} \frac{\partial v_j}{\partial \theta_i} + \frac{\partial X}{\partial \lambda_j} \frac{\partial \lambda_j}{\partial \theta_i} \right] \tag{1}$$

where X is the measured quantity, θ_1 and θ_2 represent rotations about the equatorial x and y axes (i.e., polar motion), θ_3 is an angle corresponding to UT1-UTC, and u_j, v_j, and λ_j are the cylindrical coordinates of station j. The partial derivatives of the measurements with respect to the station coordinates are available on the REGRES file. The partial derivatives of the station coordinates with respect to the Earth orientation angles are given by [10]

$$\frac{\partial u_j}{\partial \theta_1} = -v_j \cos \lambda_j \qquad \frac{\partial v_j}{\partial \theta_1} = u_j \cos \lambda_j \qquad \frac{\partial \lambda_j}{\partial \theta_1} = \frac{v_j}{u_j} \sin \lambda_j$$

$$\frac{\partial u_j}{\partial \theta_2} = v_j \sin \lambda_j \qquad \frac{\partial v_j}{\partial \theta_2} = -u_j \sin \lambda_j \qquad \frac{\partial \lambda_j}{\partial \theta_2} = \frac{v_j}{u_j} \cos \lambda_j$$

$$\frac{\partial u_j}{\partial \theta_3} = 0 \qquad \frac{\partial v_j}{\partial \theta_3} = 0 \qquad \frac{\partial \lambda_j}{\partial \theta_3} = 1 \tag{2}$$

Since the Earth orientation is a random error, for solution set two the Earth orientation angle errors are estimated as stochastic variables. A better treatment might be to consider unadjusted Earth orientation errors as stochastic variables, but this capability does not presently exist in the ODP. A priori errors of 8 nrad in the pole location and 50 nrad in UT1-UTC were assumed, corresponding to the level of error expected after 10 days of extrapolation from the last TEMPO measurement. Some correlation is expected in the errors from day to day, but little correlation between errors at separate times of measurement. Therefore, a 3.5-day correlation time was chosen as midway between two measurements taken one week apart.

For the geocentric station locations, 10-cm per coordinate errors were assumed. Thus the combination of station location error and Earth orientation error for solution set two corresponds to the equivalent station location errors used for solution set one.

Since we have broken apart the ESLE model, for this solution set the wet and dry troposphere delay errors were included using the existing partials in link REGRES. While the troposphere might be better estimated stochastically, it was desired to examine the effect of these errors separately from the Earth orientation errors and therefore only a constant 4-cm wet troposphere zenith delay error and a constant 1-cm dry troposphere zenith delay error for each station were considered.

[12] See Footnote 4.

[13] See Footnote 5.

B. Results

The RSS uncertainty results for solution set two are listed in Table 7. For these results the uncertainty contribution due to the considered ephemeris error is about 2.5 km. The considered station location error contribution is always less than the calculated uncertainty. The total uncertainty generally decreases with improved data. An exception occurs when the accuracy of the Doppler is improved from 1 mm/sec to 0.01 mm/sec with both ΔDOR and range included. In that case the increase of the considered station location error contribution still nets a small increase in the total uncertainty.

Figure 5 shows the results for the cases with 30-cm ΔDOR accuracy, 1-mm/sec Doppler accuracy, and the three different range accuracies. For these cases the calculated uncertainty is the dominant term and improves slightly with improved range accuracy. Comparison between Fig. 5 and Fig. 1 shows that the considered station location errors contribution has been reduced from 3.6 km to 0.25 km for the 10-m range case and from 18.0 km to 1.3 km for the 0.1-m range case. This shows that the largest portion of the original station location error contribution to the RSS uncertainty was due to the Earth orientation errors, which for solution set two are incorporated in the calculated uncertainty. The calculated uncertainty increased as a result, although by less than 5 percent for the cases in Fig. 5.

Figure 6 shows a comparison of the root-sum-square of the calculated uncertainty and uncertainty contribution due to station location errors for the cases from solution sets one and two that use 30-cm ΔDOR, 1-mm/sec Doppler, and 1000-m, 10-m, or 0.1-m range. This combination differs between the two sets only in the treatment of the Earth orientation errors. The more realistic treatment with estimated stochastic Earth orientation parameters produces an improved result for the more accurate data.

Figure 7 shows the RSS position uncertainty breakdown for the solution set two cases with 3-cm ΔDOR accuracy, 1-mm/sec Doppler accuracy, and the three different range accuracies. For these cases the change in range accuracy from 1000 m to 10 m or 0.1 m produces less than 3-percent change in all components. With 30-cm ΔDOR, the 0.1-m range information provides useful plane of the sky information, but that information is not competitive with 3-cm ΔDOR data. Thus, the error ellipsoid is dominated by the ΔDOR data accuracy. Figure 8 shows the B-plane uncertainty breakdowns for the case with 3-cm ΔDOR, 1-mm/sec Doppler, and 10-m range. The total uncertainties are comparable with those predicted for the MRSR mission by Konopoliv[14] assuming both radiometric and onboard optical and more conservative error modeling. This suggests that the mission requirements could be met without onboard optical data, if more accurate ΔDOR data is available, and the radio-planetary frame-tie is improved.

In the absence of ΔDOR data the orbit determination uncertainty becomes strongly dependent on the range accuracy. Improved Doppler accuracy also improves the solution, although the Doppler-only solutions are much worse than the Doppler-plus-range solutions. Figure 9 shows the RSS uncertainties for six cases: 10-m range only, 0.1-m range only, 1-mm/sec Doppler only, and 1-mm/sec Doppler with 1000-m, 10-m, and 0.1-m range. The 10-m range only solution is better than the 1-mm/sec Doppler only solution by about 40 percent. Increased range accuracy results in significantly better results. The 0.1-m range only solution, which is almost the same as the 1-mm/sec Doppler with 0.1-m range solution, is nearly as good as the solution with 30-cm ΔDOR, 1-mm/sec Doppler, and 0.1-m range shown in Fig. 5. The results without ΔDOR that have 0.01-mm/sec Doppler and either 1000-m, 10-m, or 0.1-m range (not shown in Fig. 9) have little dependence on range accuracy and are about the same as the 0.1-m range only solution.

VI. Solution Set Three

A. Error Modeling

The results presented so far are based on existing capabilities (with the exception of the data accuracies). By the mid-1990s it will be possible to have improved Earth orientation measurements, improved station locations, and troposphere corrections. In solution set three the benefits of such improvements are examined. The error modeling used in solution set three is summarized in Table 5. It has been assumed that 3-cm accuracy station coordinates will be available [11, 12]. Using a combination of weekly IRIS VLBI Earth orientation measurements and daily GPS Earth orientation rate measurements, 7-nrad UT1-UTC calibrations and 5-nrad pole location determinations should be possible [13]. It has been assumed that the use of water vapor radiometers will reduce the error in wet troposphere zenith delays to 0.5 cm [14].[15] Study of the dry troposphere delay is difficult given the current level of errors in the wet delay. Little improvement in the dry troposphere delay is envisioned, and this error has been left at 1.0 cm. Although improvements in the internal accuracy of the ephemeris are likely, they are difficult to model. Therefore the ephemeris errors used in solution set two have been maintained.

[14] See Footnote 2.

[15] S. E. Robinson, "Approximate Error Budget for Wet Delay Estimation," JPL IOM 335.4-571 (internal document), Jet Propulsion Laboratory, Pasadena, California, March 1986.

B. Results

The results for the ODP runs for solution set three are listed in Table 8. This table shows that, given the improved modeling of solution set three, the use of any one of the high-accuracy data types (0.1-m range, 0.01-mm/sec Doppler, or 3-cm ΔDOR) results in a significant decrease in the total error. This is illustrated in Figs. 10 and 11, which compare the results of solution sets two and three. In these figures, the ODP runs with 10-m range, 1-mm/sec Doppler, and 30-cm ΔDOR are designated as the "nominal" cases. For solution set one, this case had a total RSS error of 40.7 km. This result was improved to 12.3 km in solution set two due solely to the reduction in the ephemeris error contribution; the change in the Earth orientation modeling had little effect. In solution set three the total error for the nominal case is found to be essentially unchanged at 12.0 km. For the remainder of this article, this total error value of 12.0 km will be used as the benchmark by which the quality of all solutions will be judged.

Some combinations of data accuracies in set three do indeed produce a total error less than the 12.0 km of the nominal solution. Figures 10 and 11 show the error breakdown for selected combinations of data weights with the solution set two and solution set three error models. The first case shown in each figure is the nominal one with 30-cm ΔDOR, 10-m range, and 1-mm/sec Doppler. The total position uncertainty is dominated by the calculated uncertainty, with the bias acceleration error being the next largest contribution. The station and troposphere contributions for this case are reduced in solution set three but do not appreciably affect the total.

The second case in Figs. 10 and 11 differs from the nominal by using 0.1-m range along with 30-cm ΔDOR and 1-mm/sec Doppler. In solution set two the total uncertainty of 10.9 km for this case is slightly better than the nominal. The total uncertainty improves to 6.7 km in solution set three. This improvement is primarily due to the reduction in the calculated uncertainty, resulting from improved Earth orientation. The station and troposphere error contributions would be significant in solution set three if the a priori errors of these had been left at the more pessimistic solution set two level.

The third case in Figs. 10 and 11 includes 0.01-mm/sec Doppler with the nominal 30-cm ΔDOR and 10-m range. In solution set two this case has a larger total uncertainty than the nominal due to the troposphere and station error contributions. In solution set three the total of 5.1 km for this case is less than half of the nominal. The reduction in the station and troposphere components is the main reason for this improvement, but the improved Earth orientation has also made a large effect by reducing the calculated uncertainty by 50 percent.

The fourth case in Figs. 10 and 11 uses ΔDOR improved to 3 cm along with 10-m range and 1-mm/sec Doppler. The total uncertainty for this case is less than half the nominal in both solution set two and solution set three. The improvement in the troposphere contribution is responsible for the reduction in total uncertainty from 5.2 km in solution set two to 4.0 km in solution set three. The improved Earth orientation and station location accuracy have negligible effect.

The final case included in Figs. 10 and 11 uses only 0.1-m range. These results show that range is the strongest stand-alone data type of the three examined. The total uncertainty for this case is 15.3 km in solution set two, which is only 22 percent worse than the nominal case. In solution set three the total uncertainty is 7.5 km, which is 60 percent of the nominal value. The improvement from solution set two to solution set three results from both the improved Earth orientation and the reduced station location errors. The strength of this data type as a stand-alone observable may have important implications for another area of advanced study, Earth-based navigation based on optical telemetry.[16]

VII. Summary and Conclusion

It has been found that approach navigation for missions to the inner planets in the mid-1990s may benefit significantly from improved tracking data, provided that the right ascension uncertainty for the planetary ephemerides is reduced. This improved frame tie can result from improved ground surveys linking key VLBI and LLR stations, short-period pulsar observations, observations of occultations of quasars by planets, and VLBI observations during the Phobos Lander Mission and the Mars Observer Mission. Without this improved frame tie, the orbit determination accuracy is insensitive to improvements in the data accuracy. If the frame tie can be established at the 5-nrad level, an immediate improvement of a factor of three in orbit determination accuracy results (for the nominal case with 30-cm ΔDOR, 1000-m range, and 1-mm/sec Doppler). An additional factor of two improvement can then be attained by improving the ΔDOR accuracy to 3 cm.

Error model improvements studied here include improved representation of the station locations and Earth orientation errors. Orbit determination accuracy actually degrades with improved range and Doppler data when station location errors

[16] W. M. Folkner, M. H. Finger, and J. M. Davidson, "Implications of Daytime Sky Brightness for Ground-Based Optical Navigation," JPL IOM 335.3-88-114 (internal document), Jet Propulsion Laboratory, Pasadena, California, October 28, 1988.

are forced to account for Earth orientation errors. Separating the Earth orientation and the geocentric station location errors, as was done in Section IV, provides a more physically meaningful model, such that improvements in range or Doppler accuracies result in improved orbit solutions. This model also allows an examination of how improved station locations and Earth orientation, as can be provided by GPS techniques, can best be applied. Another improvement studied was the reduced troposphere error, which might be attained by GPS or water vapor radiometer techniques.

Improved ΔDOR data reduced orbit determination errors without any improvements in station location and Earth orientation calibration, although improved troposphere calibrations provided an additional 30-percent reduction in orbit determination error for cases involving 3-cm ΔDOR data. After the initial model change in which Earth orientation errors were separated from station location errors, it was found that improved range produced an improved orbit solution. In fact range was found to be by far the most useful stand-alone data type. After incorporating the improvements to the Earth orientation and station location calibrations expected in the mid-1990s, 0.1-m range was found to provide nearly a factor of two better orbit determination accuracy than 10-m range. To benefit from high-accuracy Doppler it was found that subcentimeter accuracy troposphere calibrations are required as well as the expected improvements in Earth orientation calibration and station location errors. Given these improvements, the utilization of 0.01-mm/sec Doppler can provide a factor of two improvement in orbit determination accuracy over 1-mm/sec Doppler.

These studies have been done in the absence of onboard optical data and hence do not show how improved radiometric data may complement onboard optical data. However, it has been shown that radiometric data alone can perform competitively with existing onboard optical orbit determination. This may be useful in the context of repeat missions to Mars or other inner planets when not every mission requires a camera for scientific purposes.

Acknowledgments

The authors would like to thank Jim Border, Alex Konopliv, Jim McDanell, Myles Standish, Cathy Thornton, Robert Treuhaft, and Jim Williams for helpful suggestions and discussions.

References

[1] D. C. Backer, E. B. Fomalont, W. M. Goss, J. H. Taylor, and J. M. Weisberg, "Accurate Timing and Interferometer Positions for the Millisecond Pulsar 1937+21 and the Binary Pulsar 1913+16," *Astr. J.*, vol. 90, pp. 2275–2280, 1985.

[2] O. J. Sovers, C. D. Edwards, C. S. Jacobs, G. E. Lanyi, K. M. Liewer, and R. N. Treuhaft, "Astrometric Results of 1978–85 Deep Space Network Radio Interferometry: The JPL 1987-1 Extragalactic Source Catalog," *Astr. J.* vol. 95, pp. 1647–1658, June 1988.

[3] X. X. Newhall, R. A. Preston, and P. B. Esposito, "Relating the JPL VLBI Reference Frame and the Planetary Ephemerides," in *Astrometric Techniques, Proceedings of the 109th Symposium of the IAU*, pp. 789–794, January 1984.

[4] T. P. McElrath and R. S. Bhat, "Determination of the Inner Planet Frame Tie Using VLBI Data," *Proceedings of the AIAA Astrodynamics Conference*, paper 88-4234, August 15, 1988.

[5] O. J. Sovers et al., "Radio Interferometric Determination of Intercontinental Baselines and Earth Orientation Utilizing Deep Space Network Antennas: 1971–1980," *J. Geophys. Res.*, vol. 89, pp. 7597–7607, 1984.

[6] R. Malla, "Deriving a Unique Reference Frame for GPS Measurements," *IEEE Position Location and Navigation Symposium*, pp. 177–184, 1988.

[7] C. A. Chao, "The Tropospheric Calibration Model for Mariner Mars 1971," *JPL Technical Report 32-1587*, Jet Propulsion Laboratory, Pasadena, California, pp. 61–76, 1974.

[8] X. Wu and P. L. Bender, "Carrier Phase Ambiguity Resolution and Recovery of Kauai-Maui Baseline," *EOS Trans. AGU*, vol. 69, p. 1151, 1988.

[9] W. E. Carter et al., "Difference Between the VLBI and SLR Terrestrial Reference Frames," *EOS Trans. AGU*, vol. 69, p. 1153, 1988.

[10] T. D. Moyer, "Mathematical Formulation of the Double-Precision Orbit Determination Program (DPODP)," *JPL Technical Report 32-1527*, Jet Propulsion Laboratory, Pasadena, California, May 15, 1971.

[11] S. M. Lichten, W. I. Bertiger, and E. C. Katsigris, "Sub-Meter GPS Orbit Determination and High-Precision User Positioning: A Demonstration," *Proceeding of the AIAA Astrodynamics Conference*, paper 88-4211, August 15, 1988.

[12] S. M. Lichten and J. S. Border, "Strategies for High Precision GPS Orbit Determination," *J. Geophys. Res.*, vol. 92, pp. 12751–12762, 1987.

[13] A. Freedman and J. Dickey, "Usefulness of GPS for Precise Determination of of Earth Orientation Parameters," *EOS Trans. AGU*, vol. 68, p. 1245, 1987.

[14] S. E. Robinson, "The Profile Algorithm for Microwave Delay Estimation From Water Vapor Radiometer Data," *Radio Science*, vol. 23, pp. 401–408, 1988.

Table 1. Observation schedule for MRSR study

Doppler and range data	DSS-11	DSS-44	DSS-61
First pass	July 16	July 18	July 20
Last pass	Oct. 2	Oct. 4	Sept. 30
Number of passes	14	14	13
Number of Doppler points	92	141	76
Number of range points	84	134	78
ΔDOR data	**DSS-11–DSS-44**		**DSS-11–DSS-61**
First measurement	July 19		July 18
Last measurement	Oct. 5		Oct. 4
Number of measurements	14		14

Table 2. Error modeling common to all solutions

Error source	Treatment	A priori uncertainty
Initial state		
Position	Estimated	1.0×10^{4} km per component
Velocity	Estimated	1.0 km/sec per component
Solar pressure		
G_r	Estimated	1.3×10^{-1}
G_x	Estimated	1.0×10^{-2}
G_y	Estimated	1.0×10^{-2}
Other accelerations		
Constant	Considered	1.0×10^{-12} km/sec^2 per component
Random	Estimated stochastically	1.0×10^{-12} km/sec^2 per component, $\tau = 5$ days
Mars GM	Considered	1.5×10^{-1} km^3/sec^2
Mars J2	Considered	4.4×10^{-7}
Quasar directions	Considered	5.0×10^{-9} radians per component

Table 3. Error modeling for set one solutions

Error source	Treatment	A priori uncertainty
Station coordinates	Lumped in considered ESLE	10.0 cm per component
UT1-UTC		5.0×10^{-8} radians
Earth–Mars ephemeris	Considered	1.0 × Standish covariance

Table 4. Error modeling for set two solutions

Error source	Treatment	A priori uncertainty
Station coordinates	Considered	10.0 cm per component
Earth orientation		
UT1-UTC	Estimated stochastically	5.0×10^{-8} radians
Pole direction		8.0×10^{-9} radians per component
		τ = 3.5 days
Troposphere		
Wet	Considered	4.0 cm
Dry	Considered	1.0 cm
Earth–Mars ephemeris	Considered	Standish covariance with RA offset error reduced to 5.0×10^{-9} radians

Table 5. Error modeling for set three solutions

Error source	Treatment	A priori uncertainty
Station coordinates	Considered	3.0 cm per component
Earth orientation		
UT1-UTC	Estimated stochastically	6.3×10^{-9} radians
Pole direction		4.7×10^{-9} radians per component
		τ = 3.5 days
Troposphere		
Wet	Considered	0.5 cm
Dry	Considered	1.0 cm
Earth–Mars ephemeris	Considered	Standish covariance with RA offset error reduced to 5.0×10^{-9} radians

Table 6. Data from solution set one

ΔDOR accuracy, cm	Doppler accuracy, mm/sec	Range accuracy, m	Calculated error, km	Station consider, km	Ephemeris consider, km	GM, J2 consider, km	Quasar consider, km	Bias acceleration consider, km	Total RSS error, km
-	-	1000	1308.	0.772	3.164	3.601	0.000	99.75	1312.
-	-	10	75.42	8.965	17.41	0.906	0.000	49.79	92.48
-	-	0.1	5.236	20.12	39.72	0.138	0.000	3.622	44.98
-	1	-	134.2	12.92	24.66	0.681	0.000	80.33	158.9
-	1	1000	43.53	13.32	25.68	0.474	0.000	31.68	61.12
-	1	10	22.88	18.10	35.93	0.044	0.000	13.96	48.34
-	1	0.1	5.202	20.12	39.73	0.138	0.000	3.599	44.98
-	0.01	-	55.27	60.86	106.4	4.470	0.000	40.32	140.5
-	0.01	1000	2.003	21.32	40.88	0.159	0.000	0.950	46.15
-	0.01	10	1.994	21.22	40.89	0.160	0.000	0.942	46.12
-	0.01	0.1	1.351	21.12	41.04	0.170	0.000	0.523	46.18
30	-	-	351.2	3.753	38.80	0.492	68.10	63.33	365.4
30	-	1000	10.22	0.164	38.57	0.138	1.331	7.895	40.70
30	-	10	10.02	0.199	38.84	0.161	1.310	7.219	40.77
30	-	0.1	4.642	18.03	39.72	0.137	0.372	3.260	43.99
30	1	-	93.03	10.79	41.27	0.281	9.172	49.97	114.3
30	1	1000	9.886	0.853	38.88	0.163	1.286	7.144	40.77
30	1	10	9.354	3.637	38.78	0.151	1.141	6.884	40.67
30	1	0.1	4.624	18.04	39.73	0.137	0.369	3.243	44.00
30	0.01	-	24.94	134.9	44.34	0.851	6.871	8.722	144.6
30	0.01	1000	1.975	20.67	40.79	0.154	0.0079	0.925	45.78
30	0.01	10	1.967	20.58	40.81	0.155	0.078	0.919	45.75
30	0.01	0.1	1.346	20.92	41.02	0.168	0.026	0.519	46.06
3	-	-	127.0	16.22	39.68	0.681	56.23	89.71	170.8
3	-	1000	1.856	0.287	40.16	0.103	2.305	0.770	40.28
3	-	10	1.812	0.282	40.20	0.110	2.261	0.793	40.31
3	-	0.1	1.764	1.545	40.21	0.111	2.132	0.765	40.34
3	1	-	73.53	9.266	42.43	0.612	13.33	66.07	108.8
3	1	1000	1.811	0.285	40.23	0.112	2.259	0.793	40.34
3	1	10	1.810	0.281	40.23	0.112	2.258	0.793	40.34
3	1	0.1	1.763	1.564	40.21	0.111	2.130	0.765	40.34
3	0.01	-	5.772	156.4	39.35	0.076	7.213	0.683	161.5
3	0.01	1000	1.255	8.191	39.42	0.071	1.664	0.468	40.32
3	0.01	10	1.250	8.183	39.43	0 072	1.661	0.466	40.33
3	0.01	0.1	1.095	12.30	40.05	0.107	1.139	0.389	41.93

Note: Earth orientation error is included as a 50-nrad rotation uncertainty in the 10-cm ESLE station location errors. The ephemeris covariance is from M. Standish.

Table 7. Data from solution set two

ΔDOR accuracy, cm	Doppler accuracy, mm/sec	Range accuracy, m	Calculated error, km	Station consider, km	Troposphere consider, km	Ephemeris consider, km	GM, J2 consider, km	Quasar consider, km	Bias acceleration consider, km	Total RSS error, km
-	-	1000	1307.	0.423	0.327	1.010	3.601	0.000	99.75	1312.
-	-	10	75.47	2.842	1.214	1.323	0.907	0.000	49.82	90.50
-	-	0.1	11.02	5.386	2.311	2.397	0.103	0.000	8.461	15.27
-	1	-	134.4	4.739	4.710	1.651	0.688	0.000	80.65	156.9
-	1	1000	43.89	4.584	4.261	1.723	0.483	0.000	32.02	54.72
-	1	10	24.21	4.761	3.528	2.252	0.036	0.000	14.74	29.05
-	1	0.1	10.99	5.384	2.372	2.397	0.103	0.000	8.453	15.25
-	0.01	-	91.03	36.83	91.80	5.046	3.359	0.000	51.12	143.9
-	0.01	1000	9.999	5.301	7.354	2.354	0.072	0.000	7.712	15.72
-	0.01	10	9.960	5.221	9.663	2.354	0.072	0.000	7.675	16.86
-	0.01	0.1	9.857	6.200	8.932	2.347	0.069	0.000	7.529	16.66
30	-	-	351.3	2.445	27.70	2.644	0.492	68.09	63.35	364.4
30	-	1000	10.22	0.137	2.612	2.464	0.137	1.330	7.896	13.48
30	-	10	10.02	0.141	2.562	2.477	0.161	1.310	7.219	12.92
30	-	0.1	7.707	3.262	2.568	2.472	0.136	0.912	5.841	10.85
30	1	-	93.13	3.450	6.426	2.786	0.276	9.192	50.07	106.4
30	1	1000	9.890	0.414	2.659	2.479	0.163	1.287	7.147	12.80
30	1	10	9.466	0.730	2.289	2.473	0.151	1.169	6.935	12.29
30	1	0.1	7.692	3.308	2.665	2.472	0.136	0.914	5.834	10.872
30	0.01	-	44.47	35.16	37.27	2.749	1.098	5.483	15.93	69.97
30	0.01	1000	6.500	5.301	10.59	2.457	0.115	1.082	5.022	14.66
30	0.01	10	6.497	5.293	10.52	2.456	0.115	1.080	5.017	14.61
30	0.01	0.1	6.478	5.213	9.858	2.452	0.112	1.075	4.991	14.09
3	-	-	127.3	11.45	112.8	2.707	0.676	56.73	89.91	200.9
3	-	1000	1.858	0.279	3.373	2.561	0.103	2.294	0.770	5.229
3	-	10	1.814	0.275	3.385	2.563	0.110	2.250	0.794	5.206
3	-	0.1	1.805	0.263	3.340	2.565	0.112	2.235	0.789	5.166
3	1	-	73.64	3.330	6.260	2.817	0.611	13.43	66.18	100.2
3	1	1000	1.813	0.275	3.385	2.565	0.112	2.248	0.794	5.205
3	1	10	1.812	0.274	3.380	2.565	0.112	2.247	0.794	5.201
3	1	0.1	1.804	0.264	3.341	2.565	0.112	2.235	0.789	5.166
3	0.01	-	32.78	82.93	126.1	2.690	0.892	8.305	12.75	155.2
3	0.01	1000	1.727	1.411	4.940	2.547	0.095	2.220	0.732	6.430
3	0.01	10	1.726	1.425	4.995	2.547	0.095	2.220	0.732	6.475
3	0.01	0.1	1.716	1.581	4.652	2.544	0.092	2.225	0.724	6.248

Note: Earth orientation is estimated stochastically with 8-nrad polar and 50-nrad UT1-UTC uncertainties. Station location errors are 10 cm. The zenith wet troposphere error is 4 cm. The modified ephemeris covariance includes a 5-nrad measurement of right ascension offset from the quasar frame.

Table 8. Data from solution set three

ΔDOR accuracy, cm	Doppler accuracy, mm/sec	Range accuracy, m	Calculated error, km	Station consider, km	Troposphere consider, km	Ephemeris consider, km	GM, J2 consider, km	Quasar consider, km	Bias acceleration consider, km	Total RSS error, km
-	-	1000	1308.	0.127	0.090	1.010	3.601	0.000	99.75	1312.
-	-	10	75.42	0.853	0.336	1.324	0.906	0.000	49.79	90.40
-	-	0.1	5.532	1.715	0.649	2.524	0.140	0.000	3.933	7.472
-	1	-	134.2	1.428	1.287	1.659	0.681	0.000	80.34	156.4
-	1	1000	43.54	1.378	1.167	1.732	0.474	0.000	31.68	53.91
-	1	10	22.91	1.443	0.964	2.289	0.044	0.000	13.97	26.98
-	1	0.1	5.501	1.715	0.660	2.524	0.141	0.000	3.912	7.438
-	0.01	-	66.77	10.01	13.81	5.359	2.867	0.000	50.53	85.67
-	0.01	1000	3.105	2.211	1.911	2.593	0.165	0.000	1.764	5.295
-	0.01	10	3.091	2.091	2.027	2.593	0.165	0.000	1.751	5.277
-	0.01	0.1	2.658	2.173	3.097	2.593	0.164	0.000	1.322	5.466
30	-	-	351.2	0.734	6.856	2.644	0.492	68.10	63.33	363.4
30	-	1000	10.22	0.041	0.654	2.464	0.138	1.331	7.895	13.24
30	-	10	10.22	0.042	0.641	2.477	0.161	1.310	7.219	12.68
30	-	0.1	4.892	1.318	0.363	2.528	0.138	0.399	3.484	6.671
30	1	-	93.03	1.044	1.668	2.787	0.280	9.173	49.97	106.1
30	1	1000	9.886	0.125	0.670	2.479	0.163	1.286	7.144	12.53
30	1	10	9.357	0.259	0.554	2.474	0.151	1.142	6.885	11.95
30	1	0.1	4.875	1.321	0.371	2.528	0.138	0.396	3.470	6.652
30	0.01	-	26.89	17.75	9.810	2.631	0.424	7.132	8.867	35.65
30	0.01	1000	2.981	1.990	1.940	2.583	0.153	0.201	1.635	5.101
30	0.01	10	2.969	1.885	2.024	2.583	0.154	0.199	1.628	5.084
30	0.01	0.1	2.603	2.032	2.979	2.587	0.157	0.124	1.276	5.305
3	-	-	127.0	3.608	28.78	2.706	0.680	56.27	89.71	167.9
3	-	1000	1.856	0.084	0.851	2.561	0.103	2.305	0.770	4.081
3	-	10	1.812	0.083	0.854	2.563	0.110	2.260	0.793	4.042
3	-	0.1	1.771	0.103	0.798	2.564	0.111	2.151	0.770	3.948
3	1	-	73.53	1.133	1.814	2.815	0.611	13.34	66.07	99.81
3	1	1000	1.811	0.083	0.854	2.565	0.112	2.258	0.793	4.042
3	1	10	1.810	0.083	0.853	2.565	0.112	2.257	0.793	4.040
3	1	0.1	1.771	0.104	0.798	2.564	0.111	2.150	0.769	3.947
3	0.01	-	8.585	12.35	14.60	2.522	0.110	7.063	1.117	22.29
3	0.01	1000	1.517	0.754	1.571	2.536	0.084	1.915	0.602	3.976
3	0.01	10	1.516	0.749	1.562	2.536	0.0842	1.912	0.602	3.969
3	0.01	0.1	1.505	0.713	1.567	2.540	0.089	1.845	0.594	3.930

Note: Earth orientation is estimated stochastically with 4.7-nrad polar and 6.3-nrad UT1-UTC uncertainties. Station location errors are 3 cm. The zenith wet troposphere error is 5 mm. The zenith dry troposphere error is 10 mm. The modified ephemeris covariancee is the same as that used in solution set two.

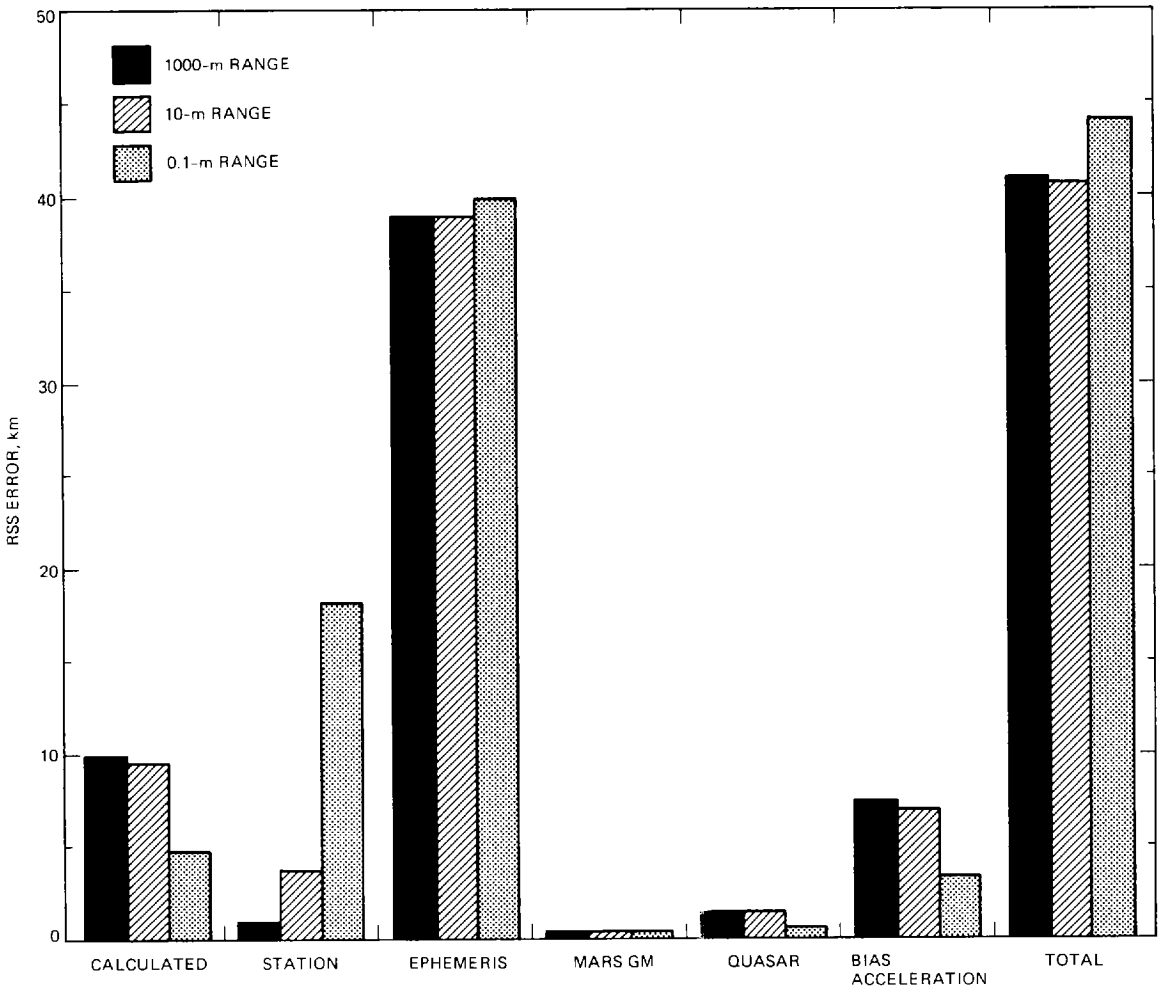

Fig. 1. RSS error breakdown for cases from solution set one with 30-cm ΔDOR, 1-mm/sec Doppler, and 1000-m, 10-m, or 0.1-m range.

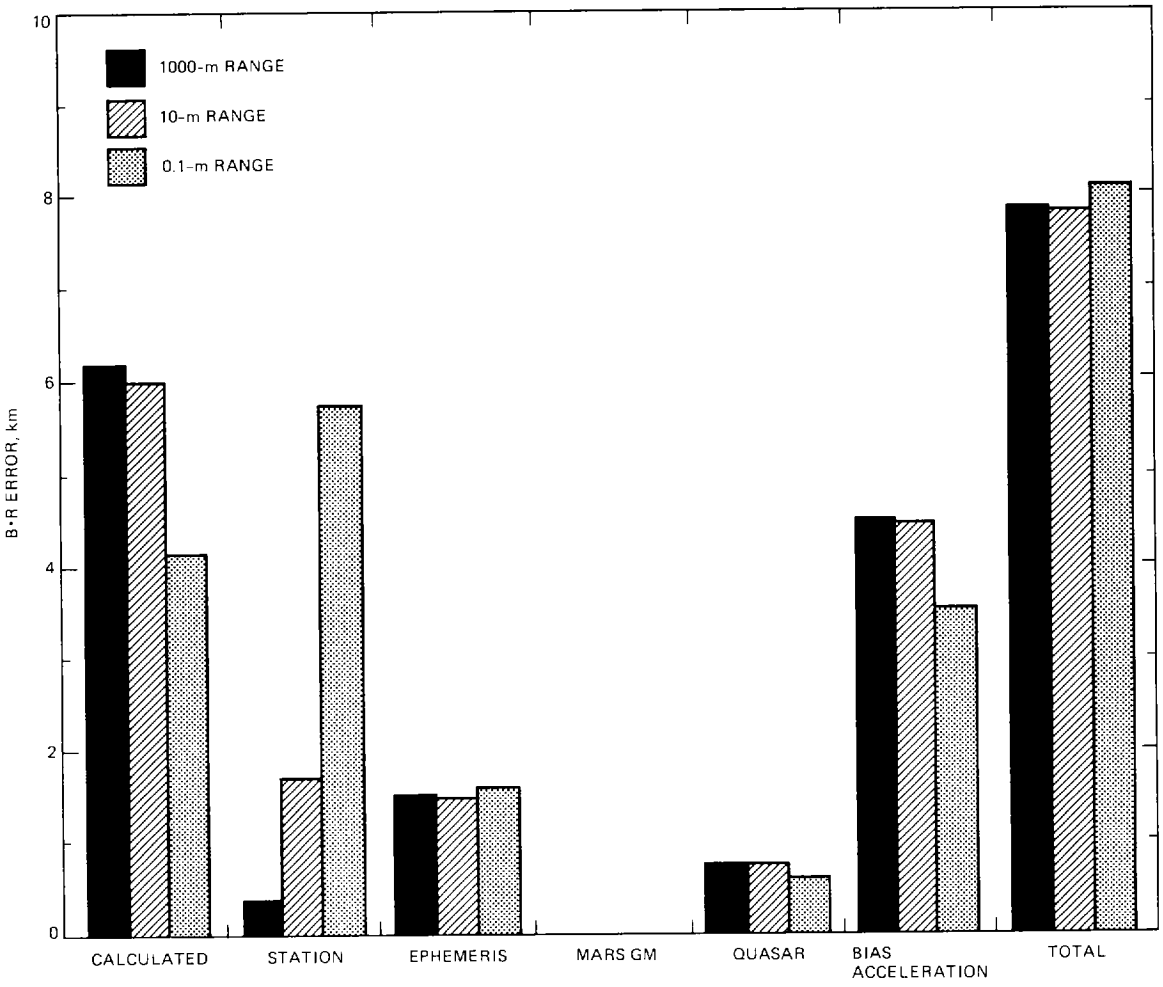

Fig. 2. $B \cdot R$ error breakdown for cases from solution set one with 30-cm ΔDOR, 1-mm/sec Doppler, and 1000-m, 10-m, or 0.1-m range.

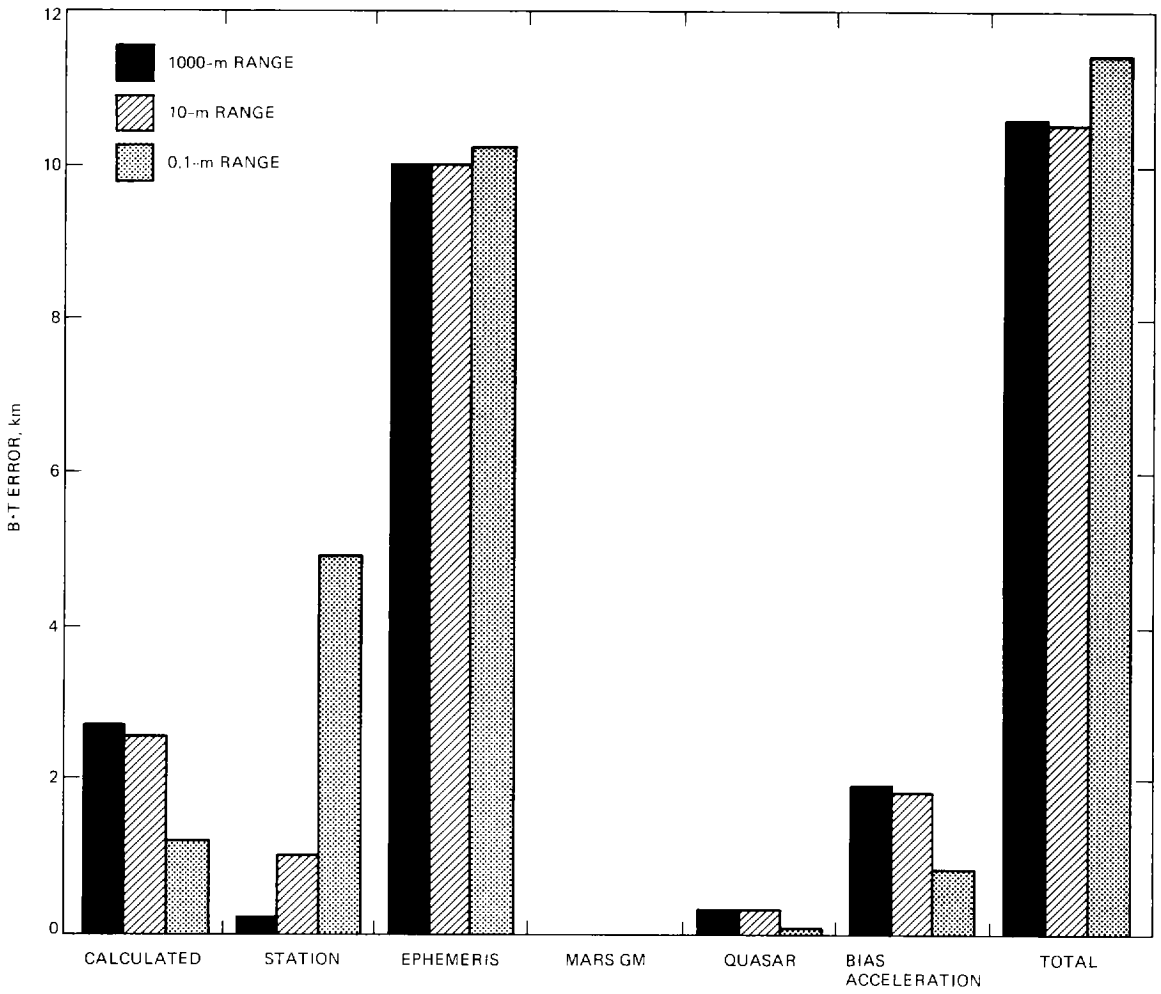

Fig. 3. *B* · *T* error breakdown for cases from solution set one with 30-cm ΔDOR, 1-mm/sec Doppler, and 1000-m, 10-m, or 0.1-m range.

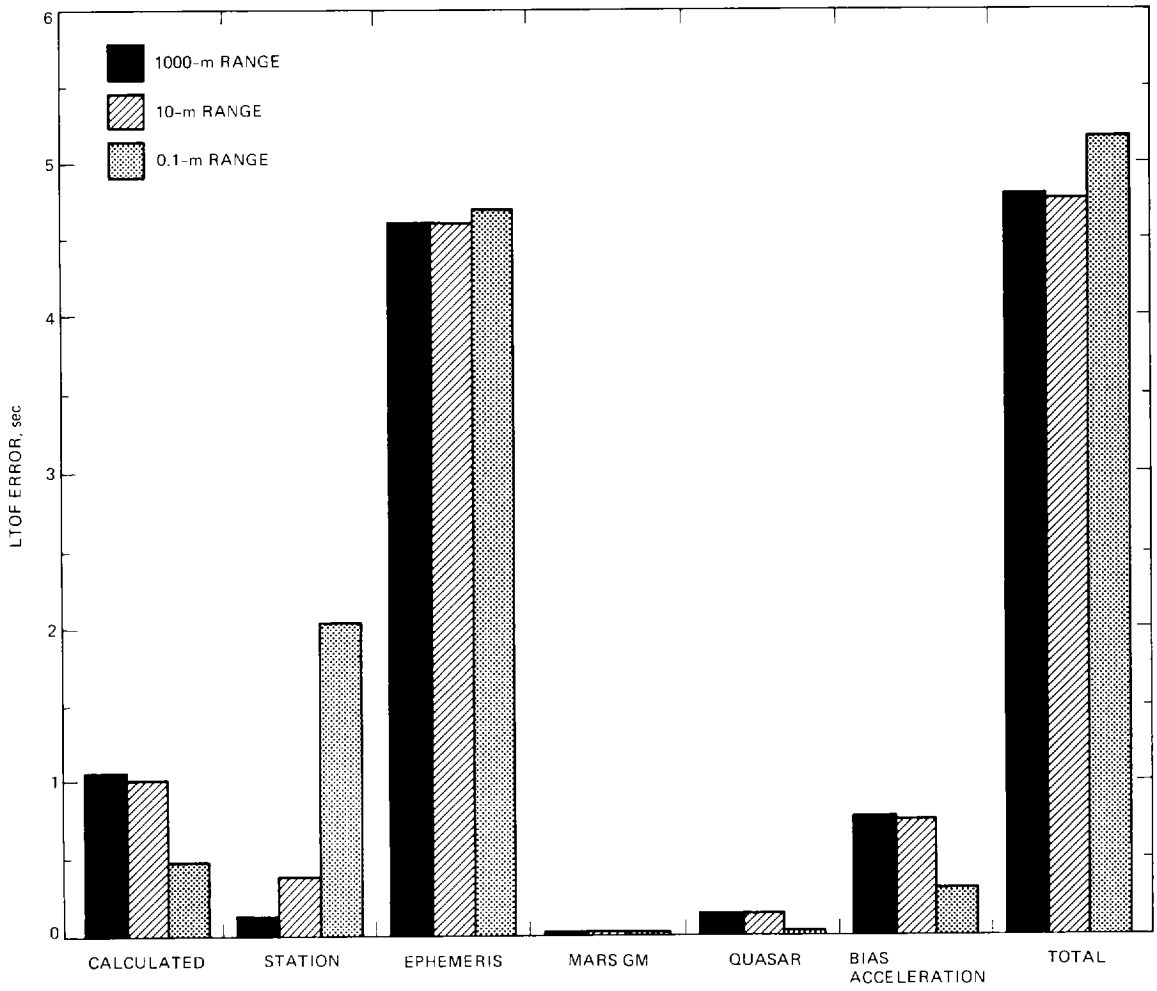

Fig. 4. LTOF error breakdown for cases from solution set one with 30-cm ΔDOR, 1-mm/sec Doppler, and 1000-m, 10-m, or 0.1-m range.

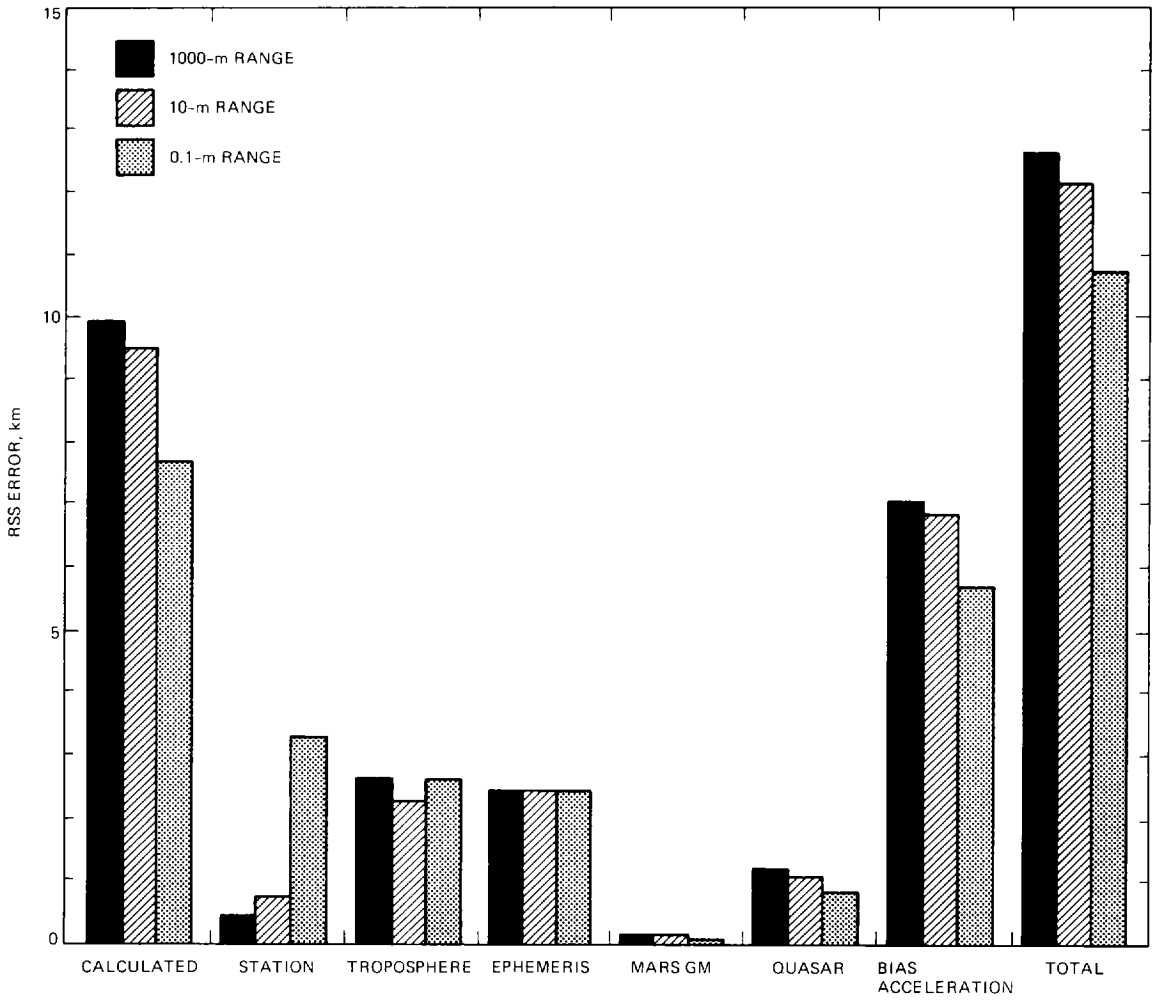

Fig. 5. RSS error breakdown for cases from solution set two with 30-cm ΔDOR, 1-mm/sec Doppler, and 1000-m, 10-m, or 0.1-m range.

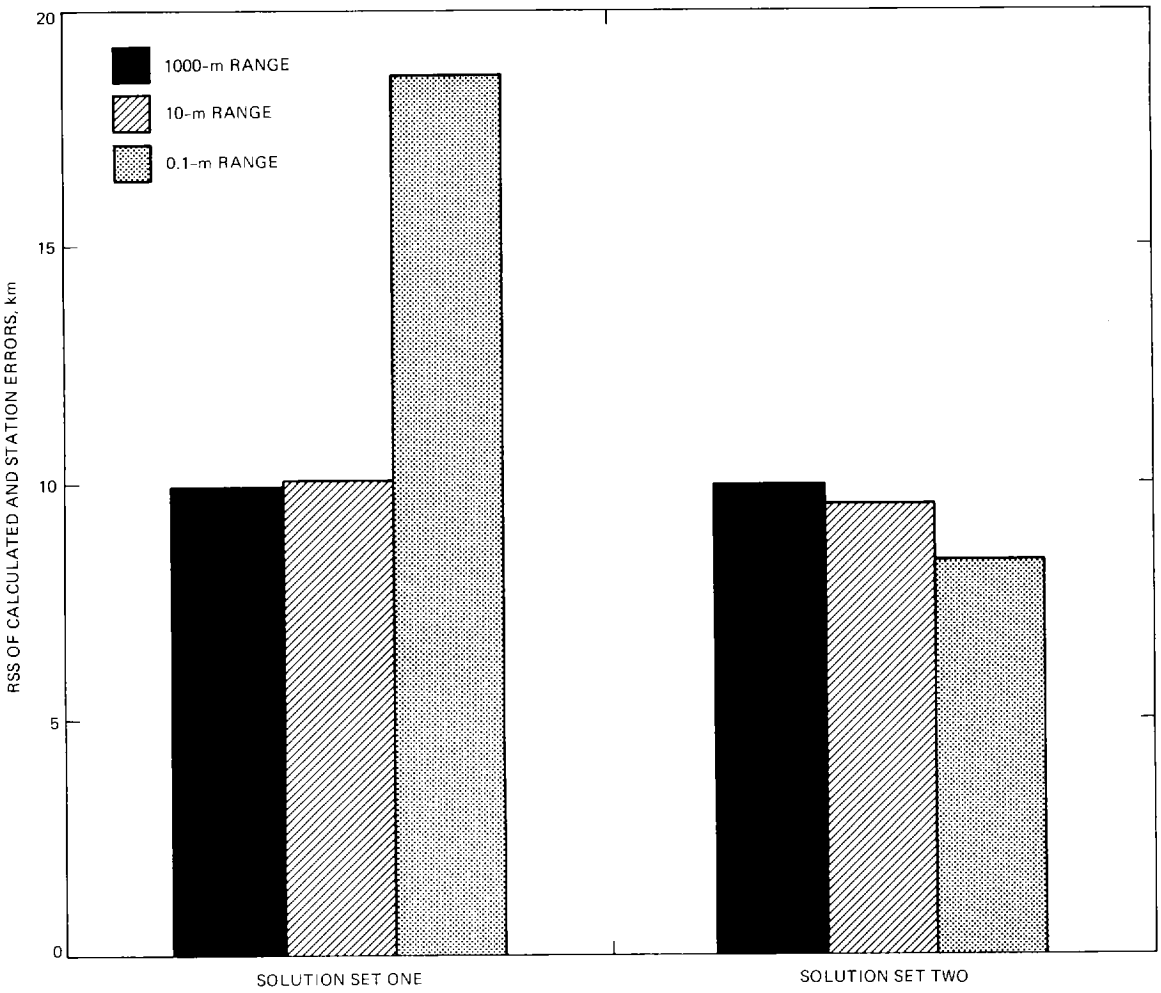

Fig. 6. Comparison of the RSS sum of calculated and station location errors for the cases in solution sets one and two with 30-cm ΔDOR, 1-mm/sec Doppler, and 1000-m, 10-m, or 0.1-m range.

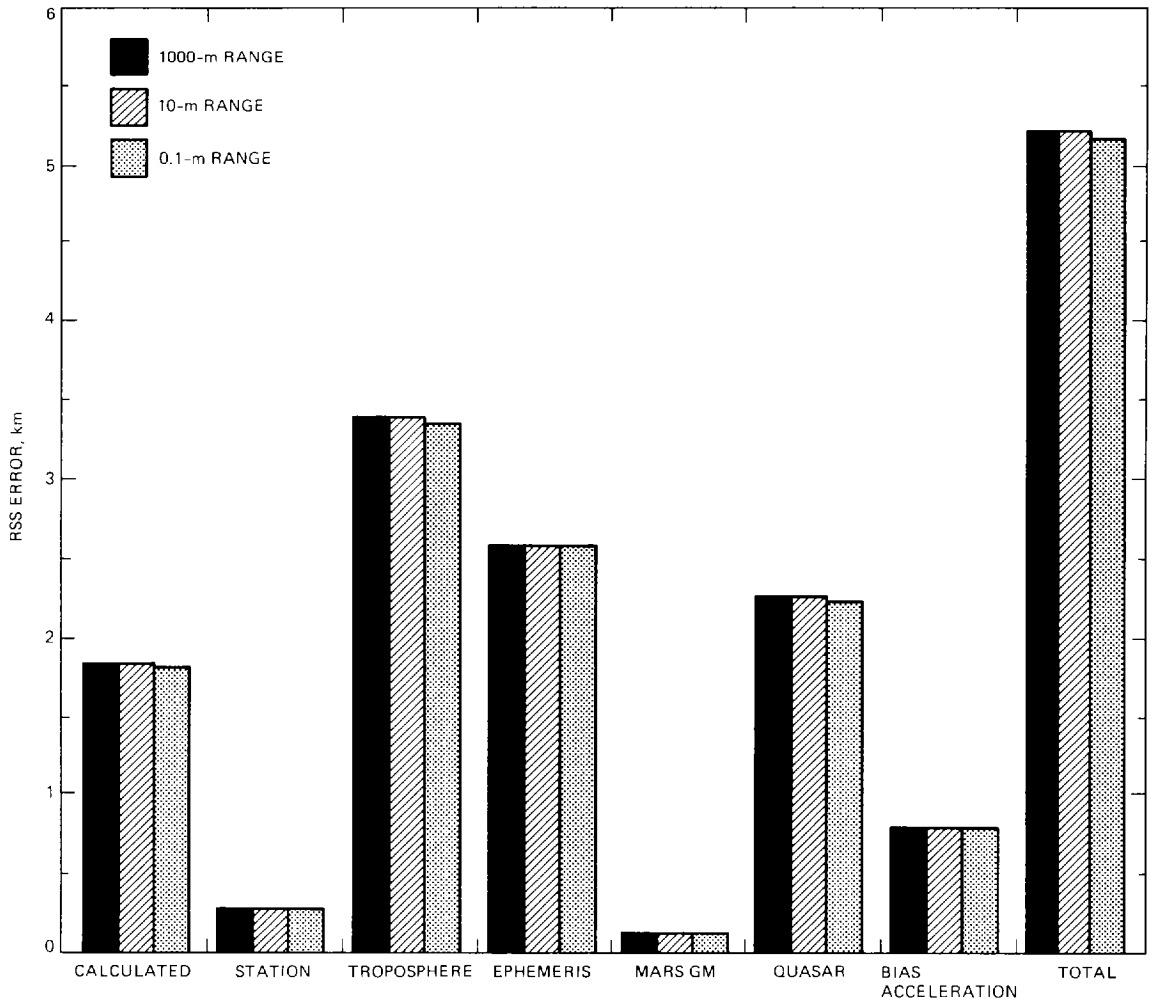

Fig. 7. RSS error breakdown for cases from solution set two with 3-cm ΔDOR, 1-mm/sec Doppler, and 1000-m, 10-m, or 0.1-m range.

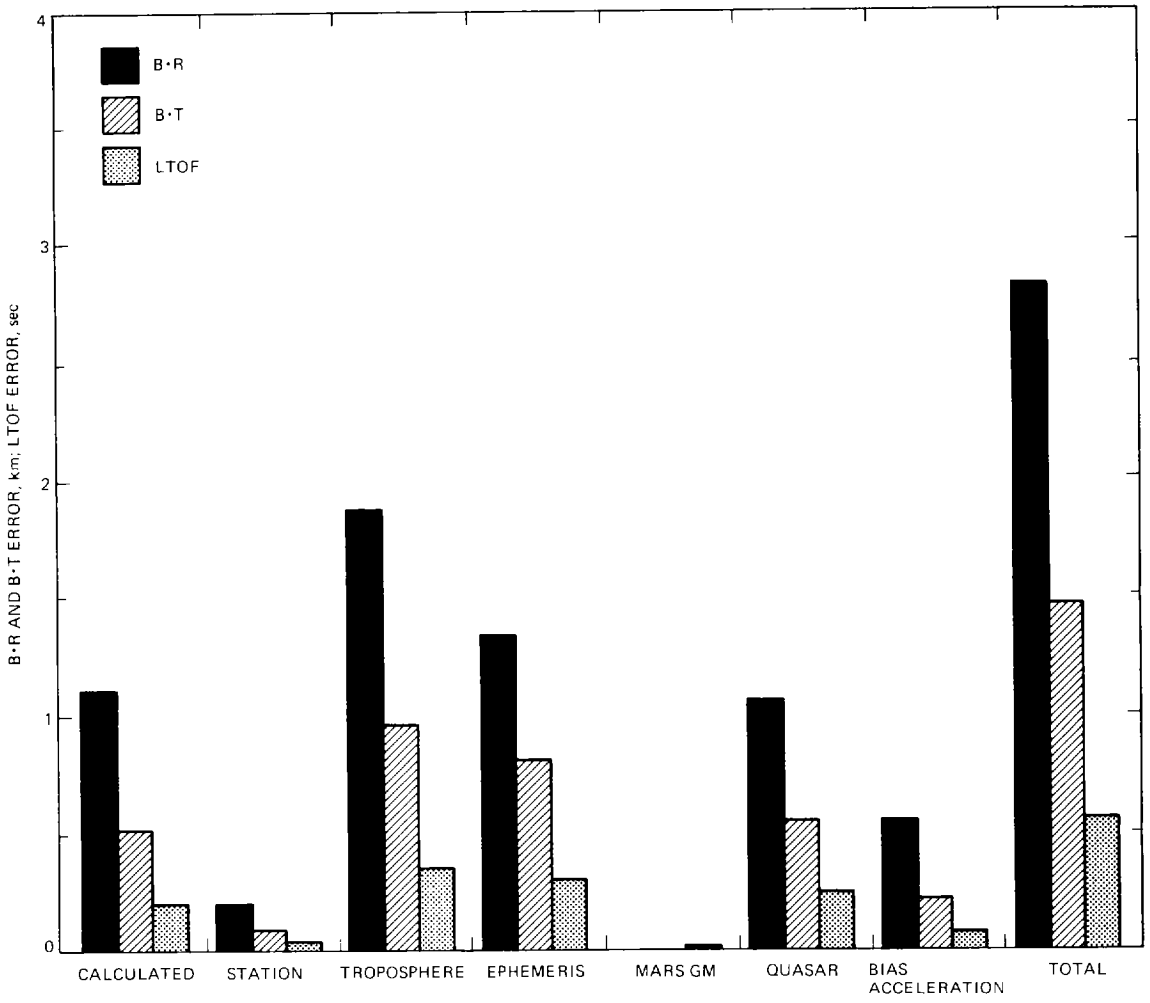

Fig. 8. B-plane error breakdown for the case from solution set two with 3-cm ΔDOR, 1-mm/sec Doppler, and 10-m range.

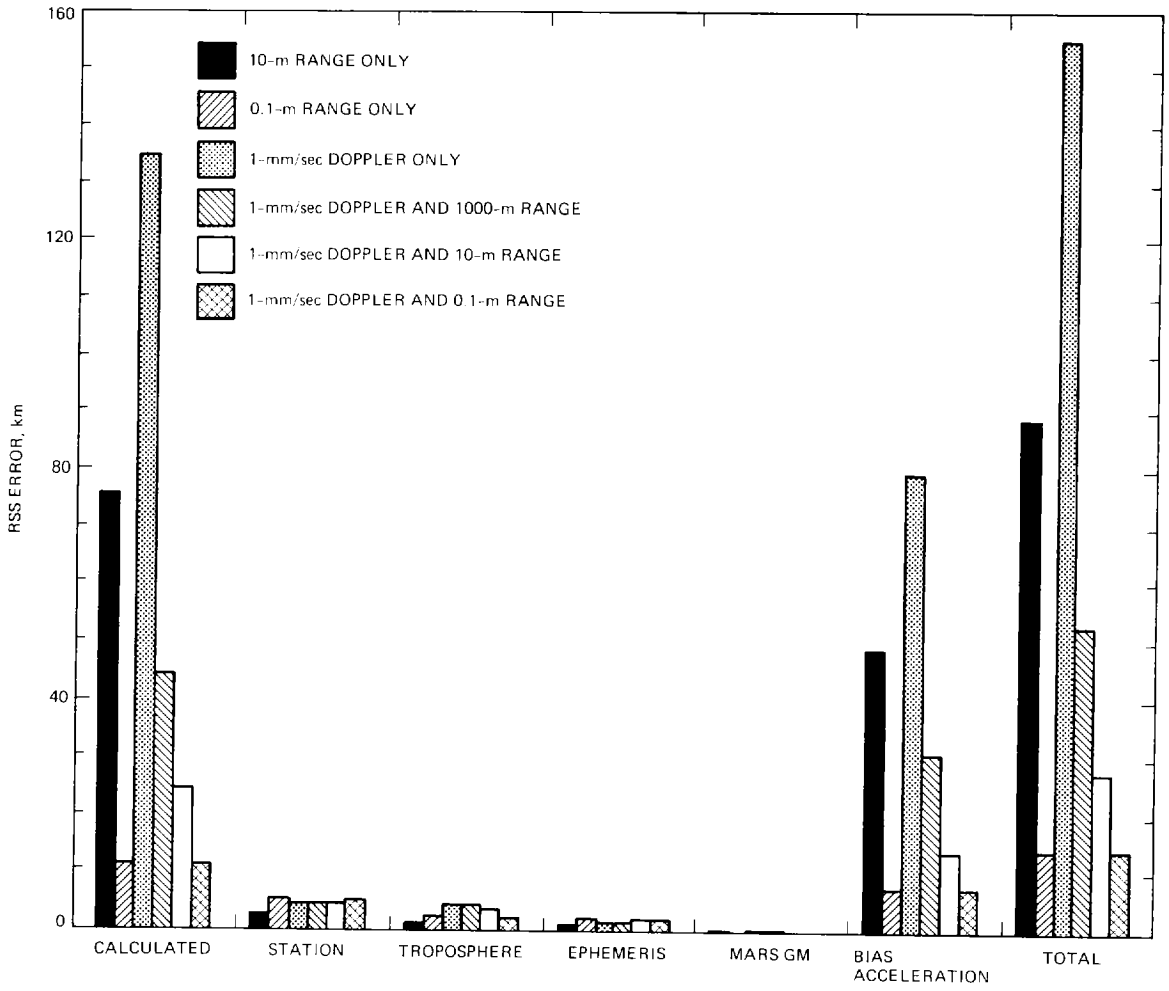

Fig. 9. RSS error breakdown for selected cases from solution set two with no ΔDOR data.

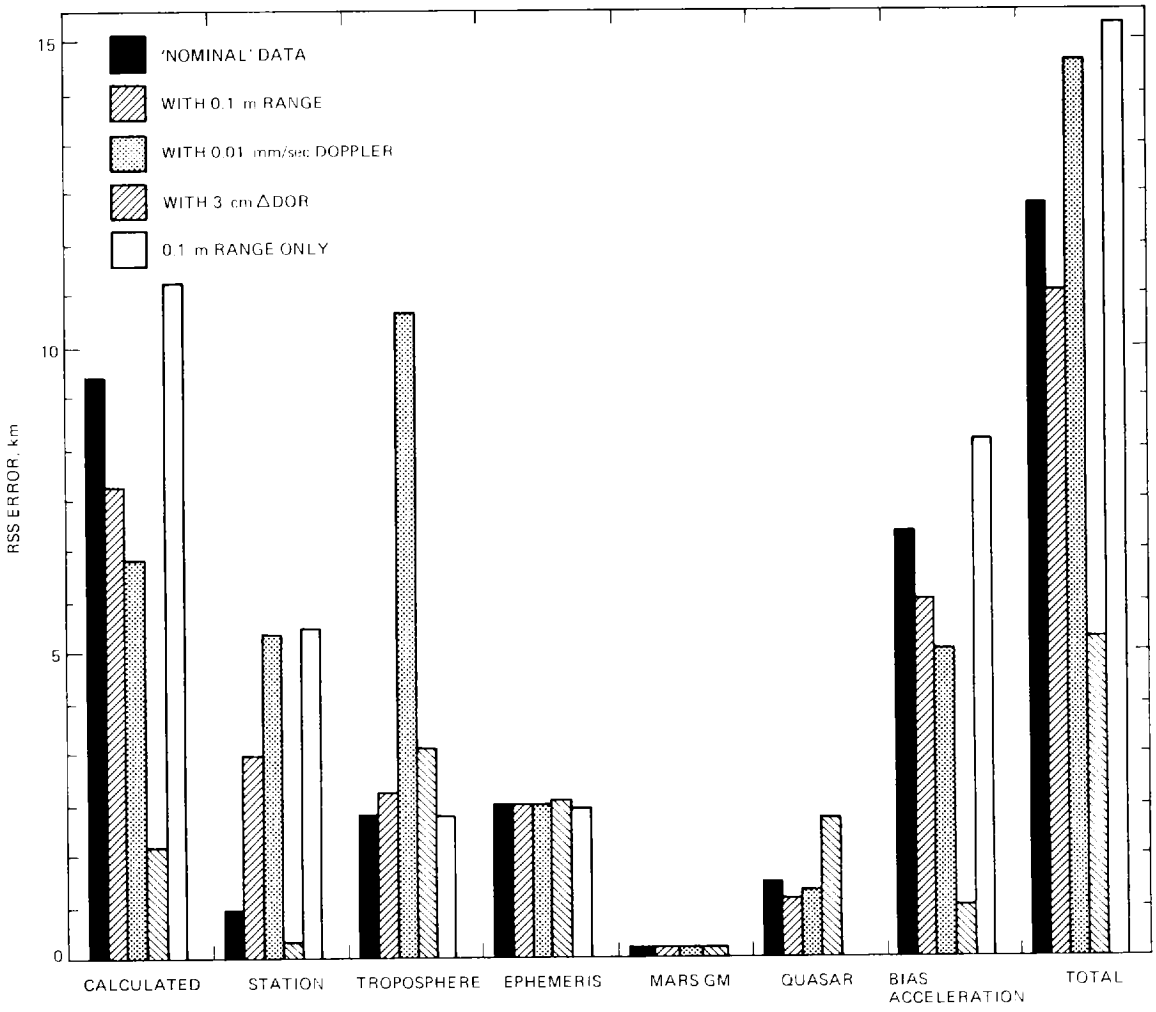

Fig. 10. RSS error breakdown for selected cases from solution set two. The nominal case uses 30-cm ΔDOR, 1-mm/sec Doppler, and 10-m range. Three of the remaining cases depart from the nominal case by the improvement of, as indicated, one of the data accuracies. The final case uses 0.1-m range only.

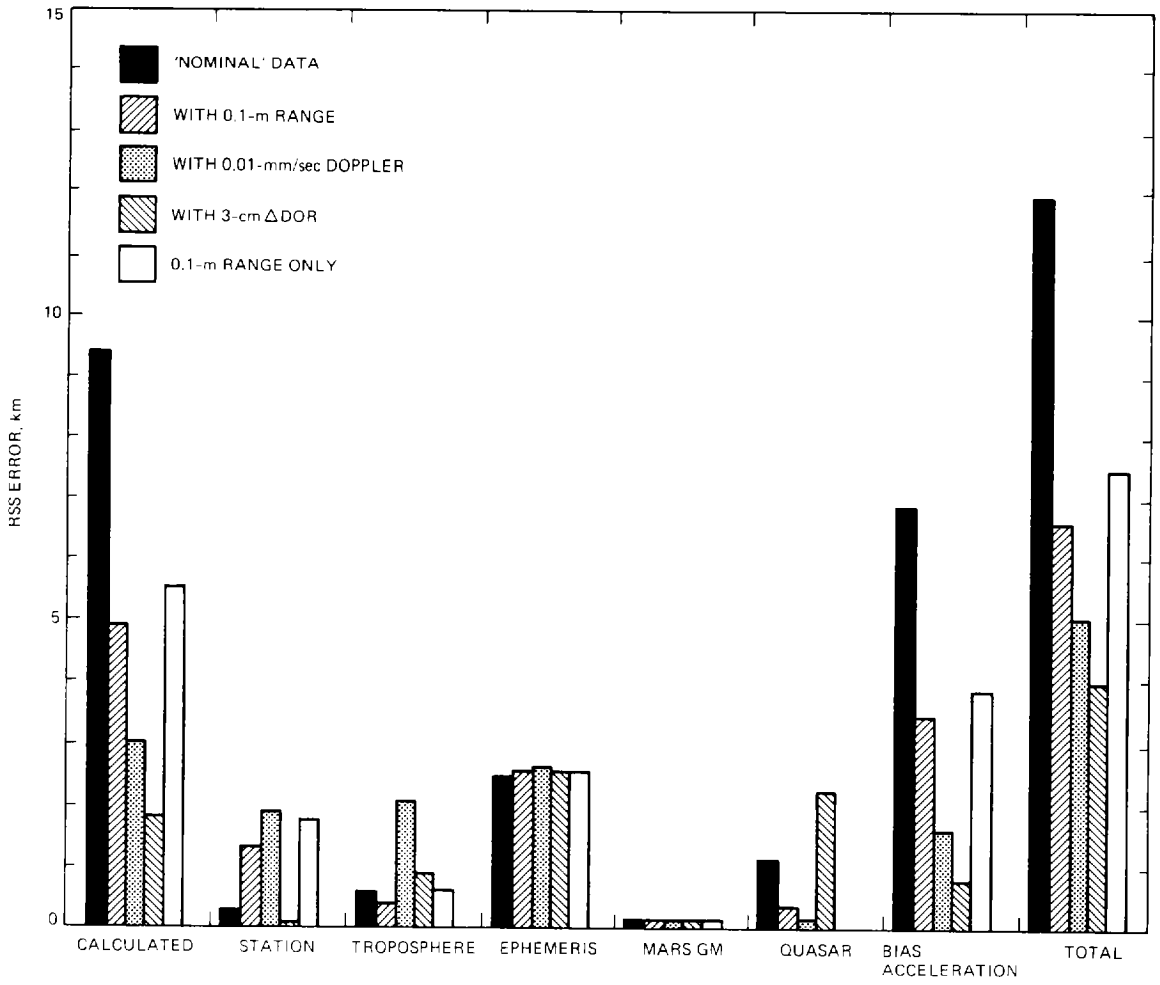

Fig. 11. RSS error breakdown for selected cases from solution set three. The data accuracy combinations are the same as in Fig. 10. The nominal case uses 30-cm ΔDOR, 1-mm/sec Doppler, and 10-m range. Three of the remaining cases depart from the nominal case by the improvement of, as indicated, one of the data accuracies. The final case uses 0.1-m range only.